frontiers | Frontiers in Materials

TYPE Original Research
PUBLISHED 30 September 2024
DOI 10.3389/fmats.2024.1484465

OPEN ACCESS

EDITED BY
Richard Drevet,
Masaryk University, Czechia

REVIEWED BY
Angela De Bonis,
Università degli Studi della Basilicata, Italy
Shanshan Shi,
University of South Carolina, United States
Rodianah Alias,
Sultan Zainal Abidin University, Malaysia

*CORRESPONDENCE
Josefina Ballarre,
jballarre@fi.mdp.edu.ar

RECEIVED 21 August 2024
ACCEPTED 17 September 2024
PUBLISHED 30 September 2024

CITATION
Kloster GA, Rivero G, Ballarre J, Herrera Seitz MK, Ceré SM and Abraham GA (2024) Innovative pH-triggered antibacterial nanofibrous coatings for enhanced metallic implant properties.
Front. Mater. 11:1484465.
doi: 10.3389/fmats.2024.1484465

Innovative pH-triggered antibacterial nanofibrous coatings for enhanced metallic implant properties

Gianina A. Kloster[1], Guadalupe Rivero[1], Josefina Ballarre[1]*, M. Karina Herrera Seitz[2], Silvia M. Ceré[1] and Gustavo A. Abraham[1]

[1]Research Institute of Materials Science and Technology, INTEMA (UNMdP-CONICET), Mar del Plata, Argentina, [2]Institute of Biological Research, IIB (UNMdP-CONICET), Mar del Plata, Argentina

Metallic stainless steel bone implants are widely used due to their excellent mechanical properties, low cost, and ease of fabrication. Nanofibrous composite polymers have been proposed as coatings to promote biocompatibility and osseointegration, thanks to their biomimetic morphology that resembles the extracellular matrix. However, critical practical issues are often overlooked in the literature. For instance, applying coatings to implants with different shapes presents a significant technological challenge, as does evaluating viable sterilization procedures for hybrid devices containing electrospun polymers. In addition, infections pose a risk in any surgical procedure and can lead to implant failure, there is a need for antimicrobial prevention during surgery as well as in the short term afterward. In this work, we propose a new and straightforward method for manufacturing nanofibrous composite coatings directly on thin cylindrical-shaped metallic implants. Poly(ε-caprolactone) (PCL) nanofibers containing bioactive glass microparticles were electrospun onto stainless steel wires and then post-treated using two different strategies to achieve both hydrophilicity and surface disinfection. To address antimicrobial properties, amoxicillin-loaded Eudragit®E nanofibers were co-electrospun to impart pH-selective release behavior in event of a potential infection. The resulting composite hybrid coatings were characterized morphologically, physically, chemically, and electrochemically. The antibacterial behavior was evaluated at different media, confirming the release of the antibiotic in the pH range where infection is likely to occur. The impact of this study lies in its potential to significantly enhance the safety and efficacy of orthopedic implants by offering a novel, adaptable solution to combat infection. By integrating a pH-responsive drug delivery system with antimicrobial coatings, this approach not only provides a preventive measure during and after surgery but also addresses the growing issue of antibiotic resistance by targeting specific infection conditions.

KEYWORDS

orthopedic implants, smart antibiotic release, electrospun nanofibers, bioglass composites, electrochemical characterization, antibacterial behavior

1 Introduction

A permanent orthopedic implant should have certain desired features, including good mechanical properties, corrosion resistance, chemical inertness, durability in harsh physiological environments, and a surface that enhances bone tissue growth, term fixation and fast bone attachment and healing (Ballarre et al., 2013; Trzaskowska et al., 2020). Metallic implants are often chosen due to their excellent combination of mechanical properties and durability compared to other materials. Additionally, they offer the required mechanical strength to withstand physical loading and sufficient elastic deformation to resist failure under cyclic physiological stress (Stewart et al., 2019). The most commonly used metals include stainless steels, cobalt-chromium alloys, titanium alloys, zirconium and tantalum (Su et al., 2018; Adhikari et al., 2018). Among these, stainless steel 316L (ASTM F138) is frequently chosen in developing countries as an implant material due to its relatively low cost, high corrosion resistance, high strength, and ease of fabrication (Katta and Nalliyan, 2019). However, it is highly recommended to apply a biocompatible and hemocompatible coating layer to enhance its properties (Trzaskowska et al., 2020).

In the last years, significant efforts have been directed towards enhancing the performance of metal implants, such as modifying the surface through the addition of bioactive ceramics, or by combining polymers and composites to increase corrosion resistance, biocompatibility and osseointegration (Jokar et al., 2016). Ideally, the coating should promote the osseointegration process while simultaneously mitigating or eliminating infections that could occur during the surgical procedures. This approach has been used in numerous studies focusing on titanium and magnesium alloys substrates employing various types of polymer coatings (such as PCL, PLA, PLGA) and fillers (including hydroxyapatite, ZnO nanoparticles, MgO-Ag, apatite) (Kiran et al., 2018; Hanas et al., 2018; Kim et al., 2017; Bakhsheshi-Rad et al., 2019; Soujanya et al., 2014; Li et al., 2012). The incorporation of electrospun nanofibers onto the implant surface, either as mono or multicomponent polymeric coatings, represents a straightforward strategy to provide implants with a biomimetic surface featuring high interconnected porosity and a large surface area-to-volume ratio (Prabhakaran et al., 2009). Indeed, electrospun membranes exhibit morphological similarities to the natural extracellular matrix (ECM), making them suitable as scaffolds for cell culture, thereby mimicking native structure and function (Kurusu and Demarquette, 2019; Liverani and Boccaccini, 2016). Consequently, the incorporation of nanofibrous coatings on metallic implants holds the potential to enhance cell adhesion and proliferation on the implant surface, and may promote and stimulate integration between the implant and native tissue, facilitating early osseointegration (Adhikari et al., 2018).

Among the different biopolymers available, poly(ε-caprolactone) (PCL) stands out as an excellent candidate for use as a polymer-based coating matrix. It possesses proven biocompatibility, biodegradability, FDA approval for clinical use, and the ability to be processed by electrospinning with benign solvents (Liverani and Boccaccini, 2016; Liverani et al., 2018). Additionally, glasses with specific composition range (with SiO_2, CaO, and P_2O_5 in their formulation) can react in physiological media and release ions that promote the formation of a calcium phosphate layer on the surface, thereby providing bioactivity and osseointegration qualities (Kim et al., 2019). Bioactive glasses (BG) have also been selected for their well-known effects on osteogenesis, angiogenesis, and sometimes their antibacterial activity (Liverani et al., 2018).

Bacterial infections pose a risk in any surgical procedure, both during implantation and post-surgery, and they are among the most common causes of unsuccessful implant procedures (Pawłowski et al., 2021). As a preventative measure, spraying an antibiotic solution on the implant before surgery is a common practice among surgeons. However, subsequent infections can still occur, with bacteria such as *S. aureus* and *S. epidermidis* being typical culprits, capable of forming biofilms (Li et al., 2018). Consequently, administration of antibiotics at the infection site may be preferable to systemic drugs, which may lead to inadequate penetration into targeted tissues and systemic toxicity, potentially causing liver complications, and generating agents resistant to antibiotics. Moreover, local drug delivery has been shown to achieve concentrations 200 times higher than systemic drug administration (Bagde et al., 2019). For instance, amoxicillin, a semisynthetic broad-spectrum antibiotic, is often incorporated into bone scaffolds due to its preventive action against *E. coli* and *S. aureus* (Bakhsheshi-Rad et al., 2018).

When an infection occurs, the microenvironment becomes weakly acidic (Tao et al., 2019), with local acidosis reaching pH values of almost 5.5 (Liu et al., 2018). Exploiting this change in local acidity as a trigger, a smart coating can be developed to release antibiotics in response to this physiological stimulus. Cicuéndez et al. (2018) designed pH-sensitive 3D hierarchical meso-macroporous scaffolds by rapid prototyping, based on a MGHA nanocomposite formed by a mesostructured glassy network with embedded hydroxyapatite nanoparticles loaded with levoflaxin which effectively combats *S. aureus* bacterial biofilms and promotes bone regeneration. In their work, the antibacterial agent was released in response to the infection's lowered pH. Furthermore, Tao et al. (2019) improved the antibacterial properties of titanium substrates using a pH-responsive multilayer film composed of alginate dialdehyde-gentamicin and chitosan, which was tested against *E. coli* and *S. aureus*.

Eudragit® EPO (EEPO) is a cationic copolymer composed of neutral methacrylic ester units and dimethylaminoethyl methacrylate (Lin et al., 2018) that dissolves at pH 5 or lower (Son et al., 2015). It is commonly used as a coating for the manufacture of pharmaceutical formulations, such as tablets or pills. Using EEPO in the form of electrospinning fibers offers advantages due to their high surface area to volume ratio for release, structural flexibility, ability to encapsulate high drug loadings (Abdelhakim et al., 2019) and the pH sensitive solubility. However, the pH-responsiveness profiles should be empirically tested for submicrometric fibers conformation, which may differ from the polymer manufacturer specifications when the product is intended to coat tablets or pills with a film (Giannetti et al., 2019).

Biomaterials intended for tissue engineering may undergo careful assessment, both *in vitro* and *in vivo*. Despite the cylindrical shape being the most suitable for *in vivo* testing the implants in rat model, most studies focus on polymeric coatings on flat metal substrates, thus limiting their utility and creating technological challenges (Omar et al., 2015). Surprisingly, there are only a few studies that assess non-flat substrate shapes. Mouthuy et al. (2015)

employed a metallic wire as electrospinning collector to mimic the hierarchical architecture of tissues such as tendons and ligaments. Dabirian et al. (2012) achieved continuous coatings of yarns or wires using nanofibers as a novel method for nanocoating of textile yarns and copper wires. However, these investigations and others (Yalcinkaya, 2019) did not specifically focus on the use of hybrid organic/metallic integral bone implants.

In this work, we propose the design of an innovative electrospinning and co-electrospinning configuration as a new and simple method for manufacturing cylindrical-shaped nanofibrous-coated implants on stainless steel substrates. Electrospun coatings based on composites of PCL with BG particles as well as co-electrospun coatings of PCL with BG and amoxicillin-loaded EEPO, were developed and fully characterized. Despite numerous studies focusing on composite materials for bone regeneration, some crucial issues in the biomedical materials field are often overlooked in the early stages of development. These include the requirement of a hydrophilic surface to improve biocompatibility and the mandatory sterilization before usage. Clinical procedures based on heat may not be suitable for several polymeric materials, as partial or total melting may destroy the nanofibrous morphology, making setting the appropriate sterilization conditions challenging. Gamma irradiation, a sterilization method frequently proposed for polymer implants, has several negative effects for PCL scaffolds, including crosslinking, degradation rate, and mechanical properties (Preem et al., 2019). In this study, two different strategies were assessed to meet both requirements in a post-processing step. On the one hand, basic hydrolysis followed by UV radiation exposure was evaluated to increase the hydrophilicity of the surface and disinfect the implant, respectively. On the other hand, a treatment based on peracetic acid/ethanol was performed on the BG-containing nanofibrous coating as an effective wet sterilization method previously proposed to inactivate viruses, fungi, and bacteria in grafts (McFetridge et al., 2004; Haimi et al., 2008), which also achieves polymer surface modification simultaneously. The resulting implants underwent morphological, physical and chemical characterization. Additionally, the effect of the coating and surface treatment on the corrosion behavior of the substrate was studied. Finally, the antimicrobial properties of the implants containing amoxicillin were evaluated in neutral and acidic pH media in contact with *E. coli* and *S. aureus*.

2 Materials and methods

2.1 Materials

2.1.1 Substrate

Stainless steel AISI 316LVM wires (Roberto Cordes S.A., Buenos Aires, Argentina) with a diameter of 1.0 mm were used as the substrate. The composition of the stainless steel was as follows: C 0.03% max, Mn 2% max, Si 0.75% max, P 0.025% max, S 0.01% max, Cu 0.5% max, N 0.10% max, Ni 13%–15%, Cr 17%–19%, Mo 2.25%–3%, with the balance being Fe. Samples were polished with SiC sheets grit 600 and then passivated in 50% v/v nitric acid solution at 50°C for 30 min, washed with distilled water and rinsed with ethanol before coating.

2.1.2 Coatings

PCL (Mn = 80,000 g mol^{-1}) and glacial acetic acid were purchased from Aldrich. For the fabrication of the composite coating, commercially available BG particles (Schott Vitryxx, nominal mean particle size 4 μm), were used. Eudragit® EPO (EEPO) was gently provided by EvonikRöhm GmbH® (Darmstadt, Germany). Amoxicillin trihydrate (AMX) was supplied by Parafarm®, Argentina.

2.2 Methods

2.2.1 PCL, PCL/BG and EEPO/AMX suspensions for electrospinning and co-electrospinning

The PCL solution (20% wt/v) was prepared by dissolving the polymer in glacial acetic acid by magnetic stirring at room temperature for 24 h. For the composite coating, 5 wt% of BG (considering weight percentage related to PCL mass) was homogeneously dispersed in the polymeric solution by constant stirring for 30 min and then sonicated for another 30 min. The potential effects of the solvent on the BG were assessed beforehand by immersing a particulate sample in glacial acetic acid (at the same ratio of bioglass as used in the experiments, without the polymer) for a maximum of 1 h with constant stirring, both with and without sonication in an ultrasonic bath for a maximum of 30 min. The morphological features and particle sizes were compared at different times using scanning electron microscopy (SEM) (JEOL, model JSM-6460 LV) after gold sputtering.

For the co-electrospinning procedure, a solution of EEPO (25% wt/v) was prepared in a DMF/ethanol mixture (1:2) and 1% AMX (w/w; weight of AMX to the weight of EEPO) was dissolved and stirred for 24 h.

2.2.2 Electrospinning and co-electrospinning process

A custom-made electrospinning setup was adapted for small-diameter metallic collectors (Figure 1A) using metallic wire substrates (1 mm diameter, 16.5 cm length) with a fixed 1,000 rpm rotation speed. PCL or PCL + BG solutions were loaded into 10 mL syringes and electrospun with an applied voltage range of 12–16 kV, a needle-target distance of 15 cm and a flow rate of 1.5 mL/h. A 18G stainless steel needle was moved translationally with a speed of 1 mm/s to ensure a complete coverage of the wires. Temperature and relative humidity were maintained at 25°C and 40% RH, respectively. The processing parameters (primarily the flow rate) were thoroughly optimized in order to obtain fibers thick-enough to encapsulate the bioglass inside (Supplementary Material).

For the co-electrospinning process, the setup was adapted (Figure 1B) so that the same 1,000 rpm rotating collector could be simultaneously coated with both PCL + BG and EEPO + AMX fibers. Both solutions were loaded into 10 mL syringes and electrospun with 18G stainless steel needles at 25°C and 40% RH for 10 min. For the EEPO + AMX solution, the processing parameters were optimized and a flow rate of 0.6 mL h^{-1}, voltage range of 17–20 kV and needle-target distance of 15 cm were used.

The resulting nanofibrous membranes based on PCL + BG were treated with two different experimental protocols to disinfect and to hydrophilize the surface. For method A, samples were immersed in

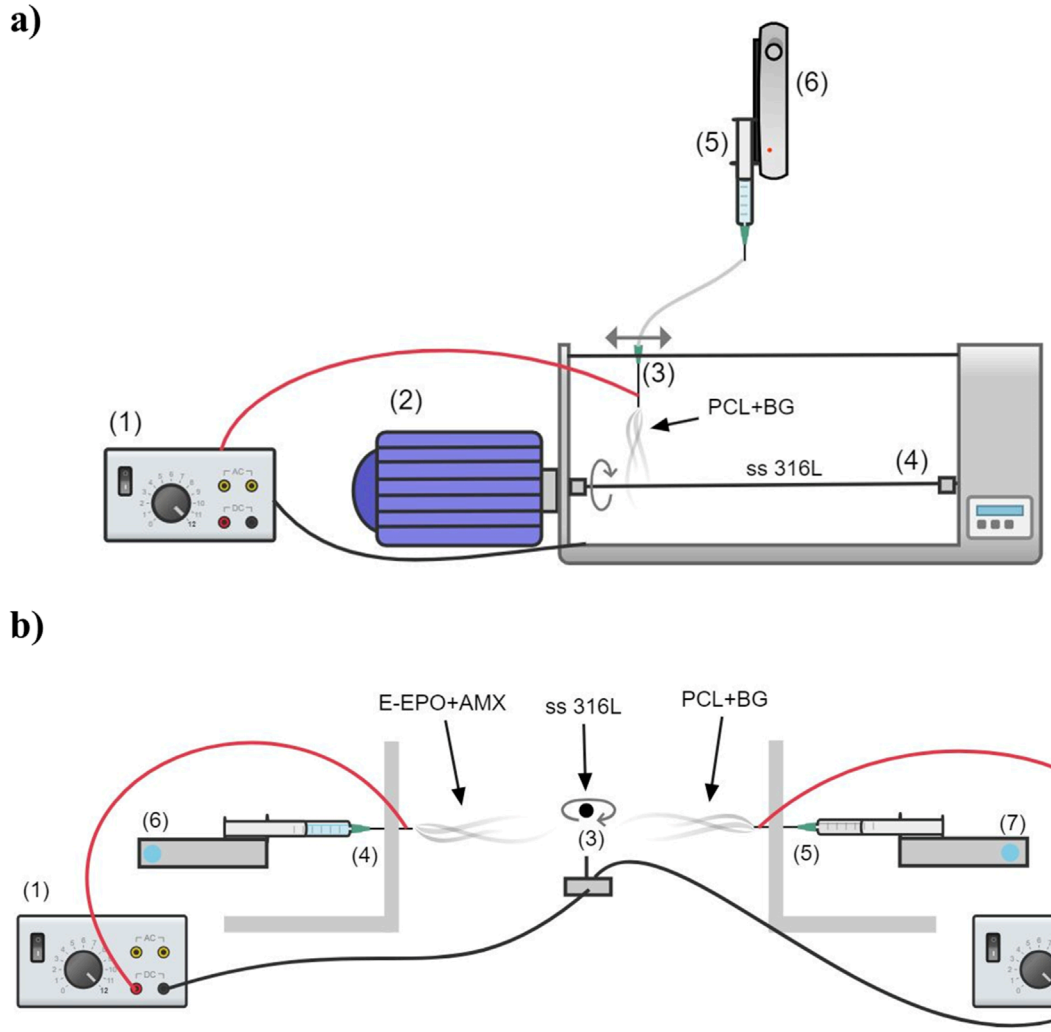

FIGURE 1
(A) Schematic representation of the electrospinning setup: high voltage power supply (1), rotational motor (2), needle with translational movement (3), metallic wire used as collector (4), syringe with polymer/BG suspensions (5), syringe pump (6). **(B)** Co-electrospinning setup used for wire recovery: high voltage power supplies (1 and 2), rotating metallic wire used as collector (3), needles and syringes with suspensions (4 and 5) and infusion pumps (6 and 7).

a solution based on peracetic acid (PA) 5,000 ppm, oxygen peroxide 0.5% v/v and ethanol 20% v/v for 15 min (Yoganarasimha et al., 2014) and then rinsed with distilled water. Method B involved basic hydrolysis with NaOH solution (5 mol/L) for 3 h (Chen et al., 2007), followed by rinsing with distilled water until neutral pH. Subsequently, exposure to ultraviolet radiation at 254 nm (UVS-28 El Series UV Lamp, Analytikjena, 8 W) was conducted during 30 min for each side at a distance of 5 cm to ensure a complete disinfection (Preem et al., 2019; Horakova et al., 2020). In the case of samples coated with PCL + BG and EEPO + AMX (co-electrospinning), the membranes were post-treated with basic hydrolysis and UV lamp according to the procedure specified above (method B).

2.2.3 Characterization

Electrospun samples were examined using a scanning electron microscope (JEOL, model JSM-6460 LV) and SEM-EDS (FEI Quanta 200) after gold sputtering. Fibers size distributions were obtained by measuring around 100 fibers from each sample with Image Pro Plus® software.

Thermogravimetric measurements of the coated wire were conducted using a TA Auto-MTG Q500 HI-Res™ instrument (TA Instruments). The measurements were carried out at a heating rate of 10°C/min under a nitrogen atmosphere (30 mL/min) from room temperature to 800°C.

Differential scanning calorimetry (DSC) thermograms of samples, both with and without the sterilization step, were acquired in a Perkin-Elmer Pyris 1 calorimeter, scanning from 0°C to 250°C at a rate of 10°C/min under a nitrogen atmosphere. The crystallinity degree χ_C was determined for the PCL-based composite coating using Equation 1 (Liverani et al., 2022):

$$\chi_C = \frac{\Delta H_m}{f \Delta H_m^o} \times 100 \quad (1)$$

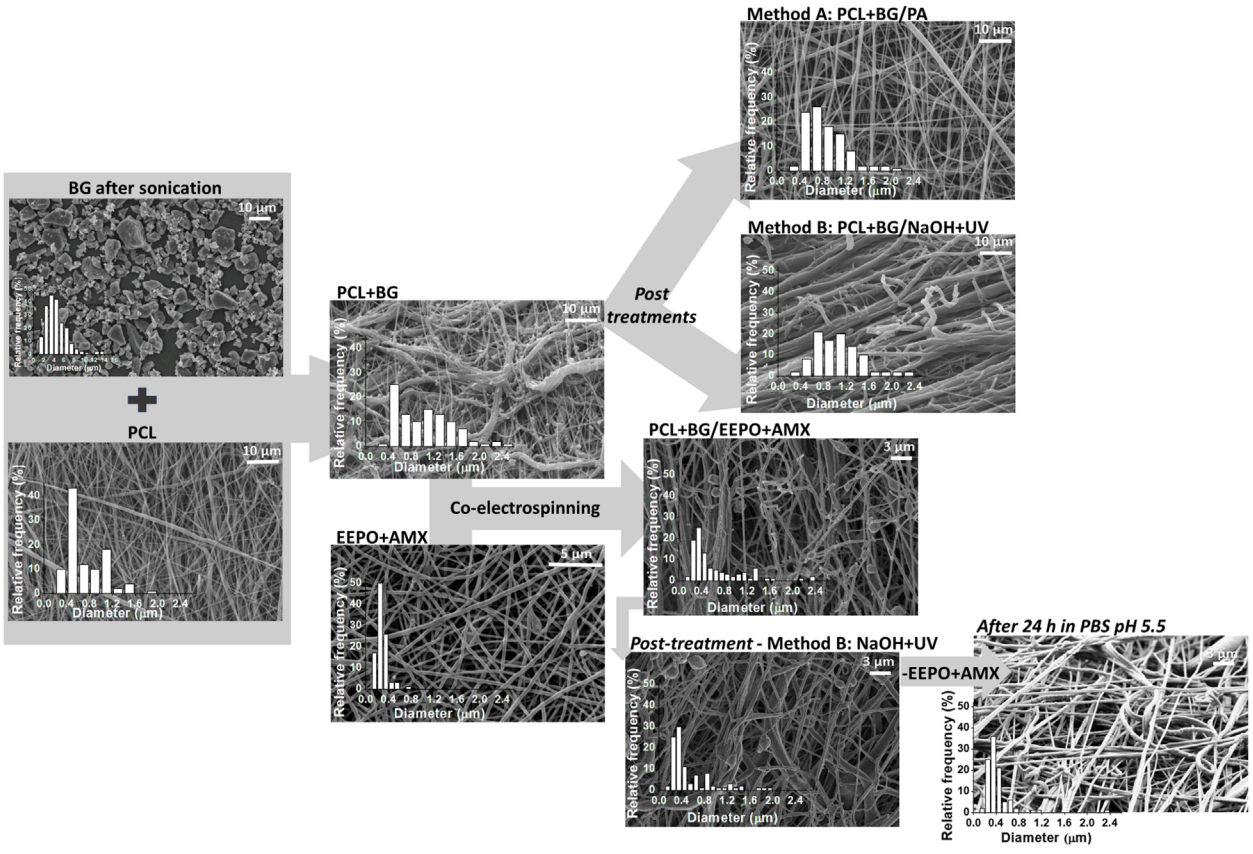

FIGURE 2
SEM micrographs of BG after sonication, PCL fibers, Eudragit + AMX fibers and the different coatings (obtained by electrospinning and co-electrospinning) before and after wet treatments.

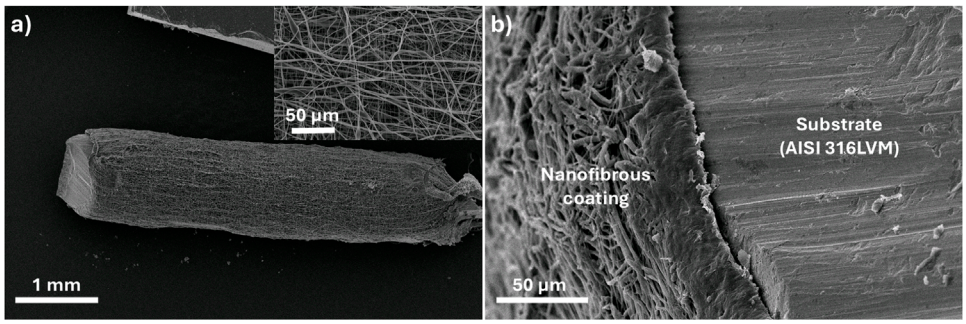

FIGURE 3
SEM micrographs of **(A)** a PCL-coated piece of wire (zoom-in shows the nanofibrous structure), and **(B)** the implant cross-section showing the substrate/coating interphase.

TABLE 1 Summary of coatings and surface treatments.

Method	Coating	Surface treatment	Sample name
Electrospinning	PCL and bioactive glasses	Method A: Peracetic acid solution	PCL + BG/PA
Electrospinning	PCL and bioactive glasses	Method B: NaOH solution + UV radiation	PCL + BG/NaOH + UV
Co-electrospinning	PCL and bioactive glasses/Eudragit E and amoxicillin	Method B: NaOH solution + UV radiation	PCL + BG/EEPO + AMX/NaOH + UV

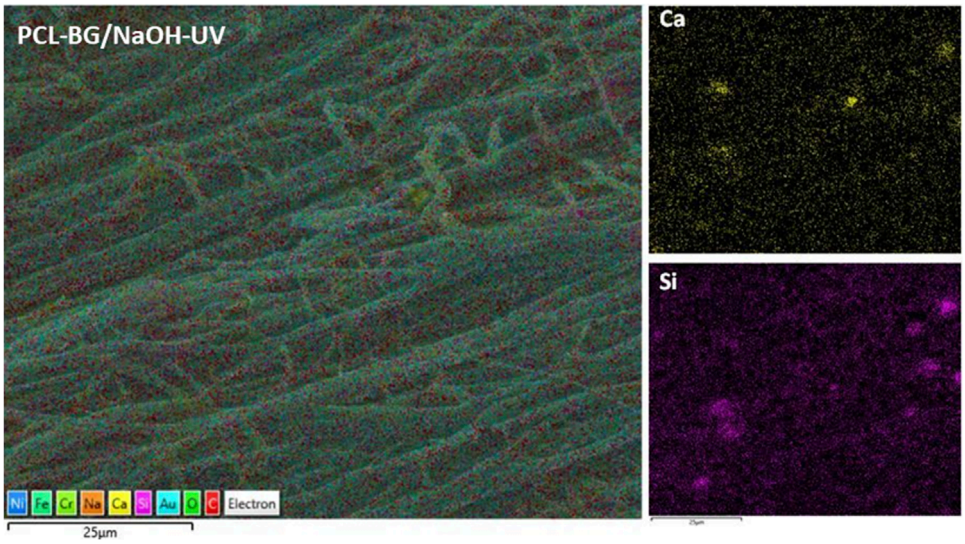

FIGURE 4
EDX qualitative mapping of PCL-BG-NaOH-UV coating.

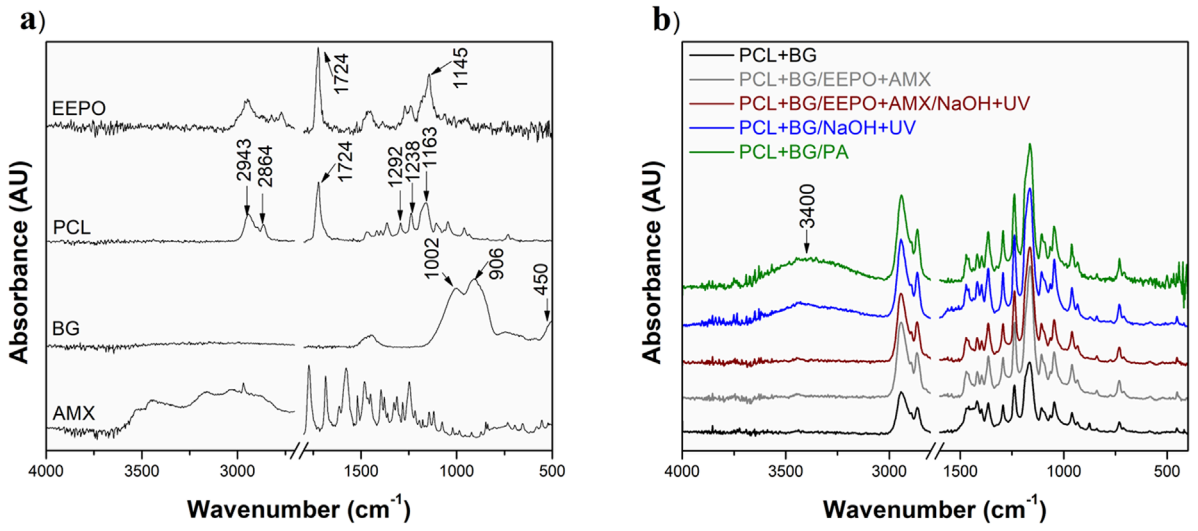

FIGURE 5
FTIR-ATR spectra of **(A)** the individual components and **(B)** the composite coatings before and after the surface treatments.

where ΔH_m is the melting enthalpy obtained in J/g, f is the mass fraction of PCL and ΔH_m^o is the theoretical melting enthalpy of a 100% crystalline PCL sample (134.9 J/g).

Fourier Transform Infrared (FTIR) spectra of the BG, PCL, EEPO, AMX and the different coatings were recorded using the attenuated total reflectance method (ATR) using a Thermo Scientific® Nicolet 6,700 Fourier transform infrared spectrometer. The spectra were collected over a range of 500–4,000 cm^{-1} with a resolution of 2 cm^{-1} and each spectrum was averaged over 64 scans.

Contact angle measurements were conducted by triplicate on the surface of flat samples to analyze the effect of the surface treatment. While morphology influences the absolute values of contact angles, comparative measurements on the flat counterparts can provide indications of the efficiency of the post-treatment. A droplet of distilled water (5 µL) was deposited and measured after 1.5 min with a goniometer (Ramé-Hart Co.; USA) and analyzed by using the Ramé-Hart software.

The AMX content in EEPO fibers was quantified by UV-vis spectroscopy in a DLAB SP-UV1000 spectrometer, monitoring the peak at 230 nm (Bakhsheshi-Rad et al., 2018), using a 0.4% w/v solution of EEPO in PBS at pH 5.5 as blank. Samples of EEPO + AMX treated with Method B were dissolved in PBS buffer at pH 5.5 and the drug content was calculated as the percentage of the loaded AMX relative to the polymer content, by using a calibration curve (R^2 = 0.991) built in a similar media. The encapsulation efficiency

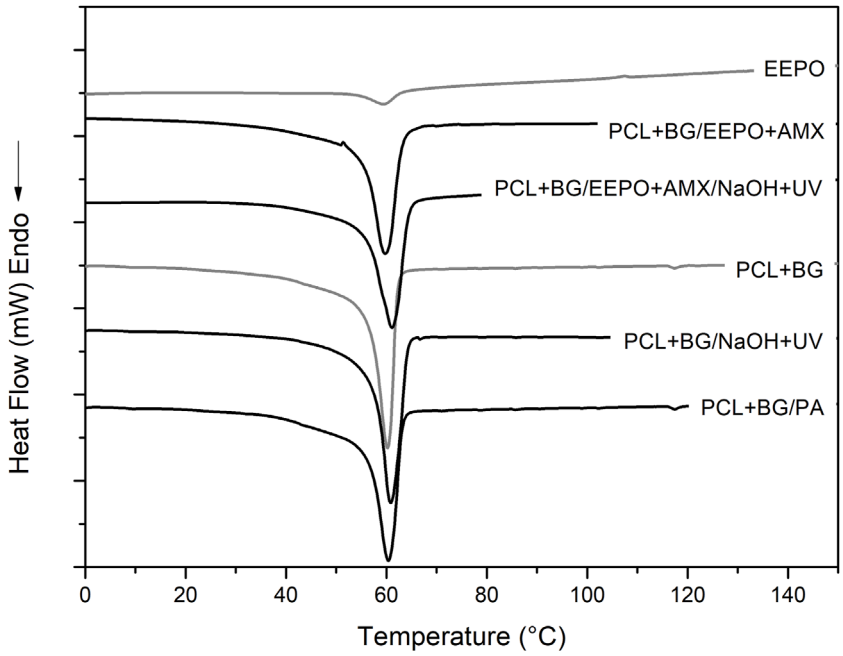

FIGURE 6
DSC thermograms of EEPO and the coatings with different compositions, before and after wet treatments.

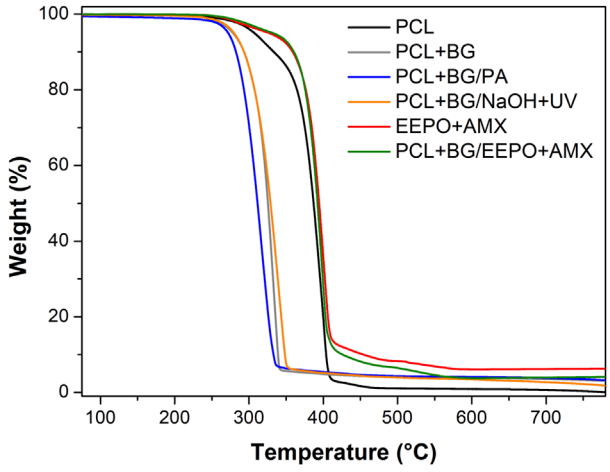

FIGURE 7
TGA curves of the polymeric coating with and without 5 wt% of BG, the PCL + BG coating with the surface treatments (PA and NaOH + UV), the EEPO + AMX coating and the co-electrospinning sample.

(%) was determined by comparing the experimental AMX content with the drug content incorporated in the pristine fluid.

The antibacterial behavior of the co-electrospinning samples with and without amoxicillin was evaluated against *S. aureus* (Gram-positive) and *E. coli* (Gram-negative) using the relative bacterial assay method in lysogeny broth (LB) medium at pH 7 and 5. Subsequently, the bacterial optical density (OD) at 600 nm of 2 mL was measured using a spectrophotometer at (6, 24 and 48 h). The experiment was conducted by duplicate after exposing the samples to UV light at 254 nm for 1 h to disinfect them.

Electrochemical assays of the bare substrate and coated samples with PCL + BG with and without post-treatments were performed using a GAMRY Ref 600 electrochemical unit (Gamry, USA) with a conventional three-electrode cell. A saturated calomel electrode (SCE) was used as a reference electrode, a platinum wire as a counter electrode and the stainless-steel wire, either with or without the coating, was used as the working electrode. Studies were conducted in simulated body fluid (SBF) (Kokubo and Takadama, 2006) at 37°C. Electrochemical impedance spectroscopy (EIS) tests were recorded around the open circuit potential (OCP) with an amplitude of 0.015 V rms sweeping frequencies ranging from 20,000 to 0.05 Hz. Polarization curves were obtained from −0.05 vs. OCP to 0.7 V vs. SCE at a sweep rate of 0.001 V s^{-1}. Previous to electrochemical assays, OCP was measured until its stabilization. The assays were conducted by duplicate or until reproducible results.

2.2.4 Statistical analysis

To analyze the effect on the means of BG diameter as a function of sonication or stirring time, and the means of fiber diameter as a function of surface treatment, a one-way analysis of variance (ANOVA) was conducted ($\alpha < 0.05$), with Tukey's posterior test. The fiber diameter variable was transformed to $\log_{10}$ to meet the assumption of normally distributed residuals in the ANOVA analysis. The effect of the surface treatment on the diameter of the fibers obtained by co-electrospinning was analyzed using Generalized Linear Models (GLM) with a gamma distribution.

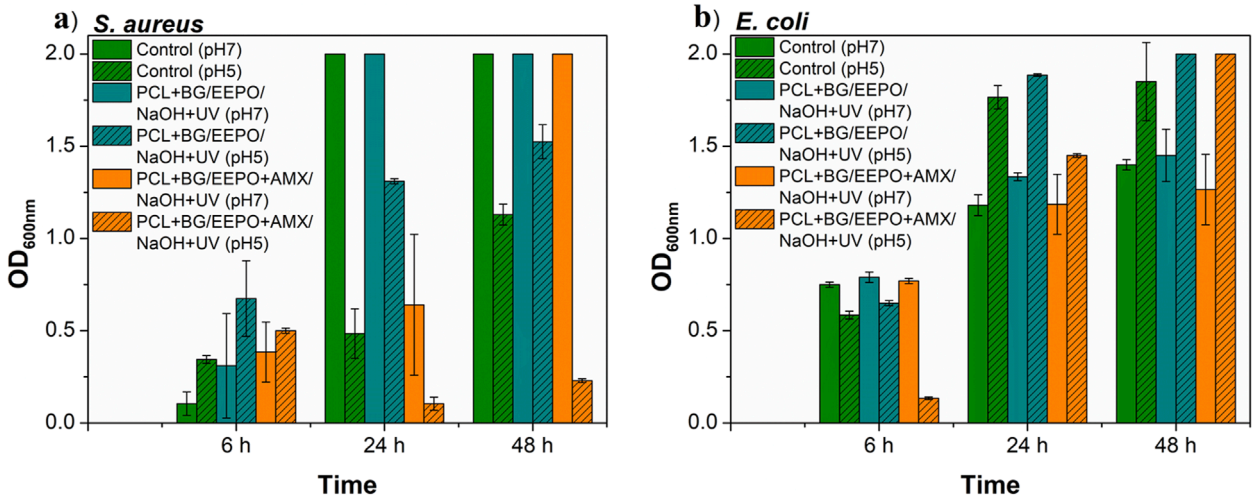

FIGURE 8
Antibacterial activity of co-electrospinning coating with and without AMX against **(A)** *S. aureus* and **(B)** *E. coli*.

3 Results and discussion

3.1 Composite fibrous coating preparation

Before fibrous composite nanofibers processing, the effect of glacial acetic acid solvent on BG particles was studied, and the maximal length of the irregular shaped particles was compared for different times of stirring or sonication (Supplementary Figure S1). Particle diameters followed a gamma distribution, almost without variation (for stirring, ANOVA $F_{(6,1393)} = 1.50$, p-value = 0.17; for sonication, ANOVA $F_{(5,1182)} = 1.8$, p-value = 0.11), and the surface did not display any noticeable break or change (Figure 2 – BG after sonication). Similar results were reported by Liverani et al. (2018) when using a mix of acetic acid and formic acid, as only slight morphological modifications with no alterations in particle size in the BG were observed.

After optimizing the processing parameters, fibrous composite membranes were successfully electrospun using both simple and co-electrospinning configurations. The diameter of PCL-BG fibers was tuned to ensure that BG particles remain inside after wet post-treatments (Supplementary Material). The coated implants could be easily cut with regular pliers after processing. Remarkably, the nanofibrous coating exhibited excellent coverage, suitable adhesion, and no delamination was observed (Figure 3). However, a partial preferential orientation of certain fibers can be noted, as a result of the small diameter of the rotational collector and the rotation speed.

3.2 Characterization and surface modification of the coatings

Different coatings and post-treatments were assessed. Table 1 summarises the different coatings and the surface-modification protocols.

Both surface modification methods effectively managed to change the surface polarity, as the contact angle for the hydrophobic PCL + BG sample (125.0° ± 6.9°) was reduced with PA treatment (62.1° ± 6.3°) and the water drop was immediately absorbed (Liverani et al., 2022) when using NaOH-UV. The effect of the surface treatment on the morphology and the fibers size distributions was assessed by SEM analysis. The SEM images in Figure 2 summarize the different coatings compositions and surface treatments. For coatings composed of only PCL-based fibers, the mean diameter for the untreated composite sample was 1.04 µm while the PA and NaOH-UV treatments led to average values of 0.86 µm, and 1.06 µm, respectively. ANOVA analysis showed statistically significant differences in the fiber diameters with the different surface treatments ($F_{(2,297)} = 6.11$; p-value = 0.0025; Tukey´s pairwise contrasts: PCL-BG vs. PCL-BG-PA $p = 0.034$; PCL-BG vs. PCL-BG-NaOH $p = 0.664$; PCL-BG-PA vs. PCL-BG-NaOH $p = 0.0025$). The basic-treatment (Figure 2: PCL + BG/NaOH + UV) led to rougher surfaces and certain fiber breakage, but the fiber diameter was not significantly altered, in accordance with the behavior reported by Yew et al. (2018). Although no evident changes in the fiber surfaces had been previously reported after acid-mediated hydrolysis (Yoganarasimha et al., 2014), the formation of bigger and denser fibers with basic treatment have been detected before (Chaiarwut et al., 2021; Bhaskaran et al., 2019).

In general, the mean diameter value for PCL + BG fibers is larger than for EEPO + AMX membrane. SEM images and fiber diameter size distribution of the co-electrospun membrane are shown in Figure 2 (PCL + BG/EEPO + AMX). After the wet surface treatment, no significant difference in the mean diameter of the fibers was noted (GLM: $t = -1.11$ $p = 0.26$). Micrographs showed fibers with a smooth surface with some beads. The co-electrospun membrane was immersed in PBS pH 5.5 media, where the EEPO + AMX fibers were effectively dissolved, as expected. Remarkably, the PCL nanofibrous structure was preserved, with no significant variation in the overall fiber diameter distribution. This experience ensures the structural integrity of the co-electrospun membrane, even after an eventual dissolution of one of the types of fibers that compose it.

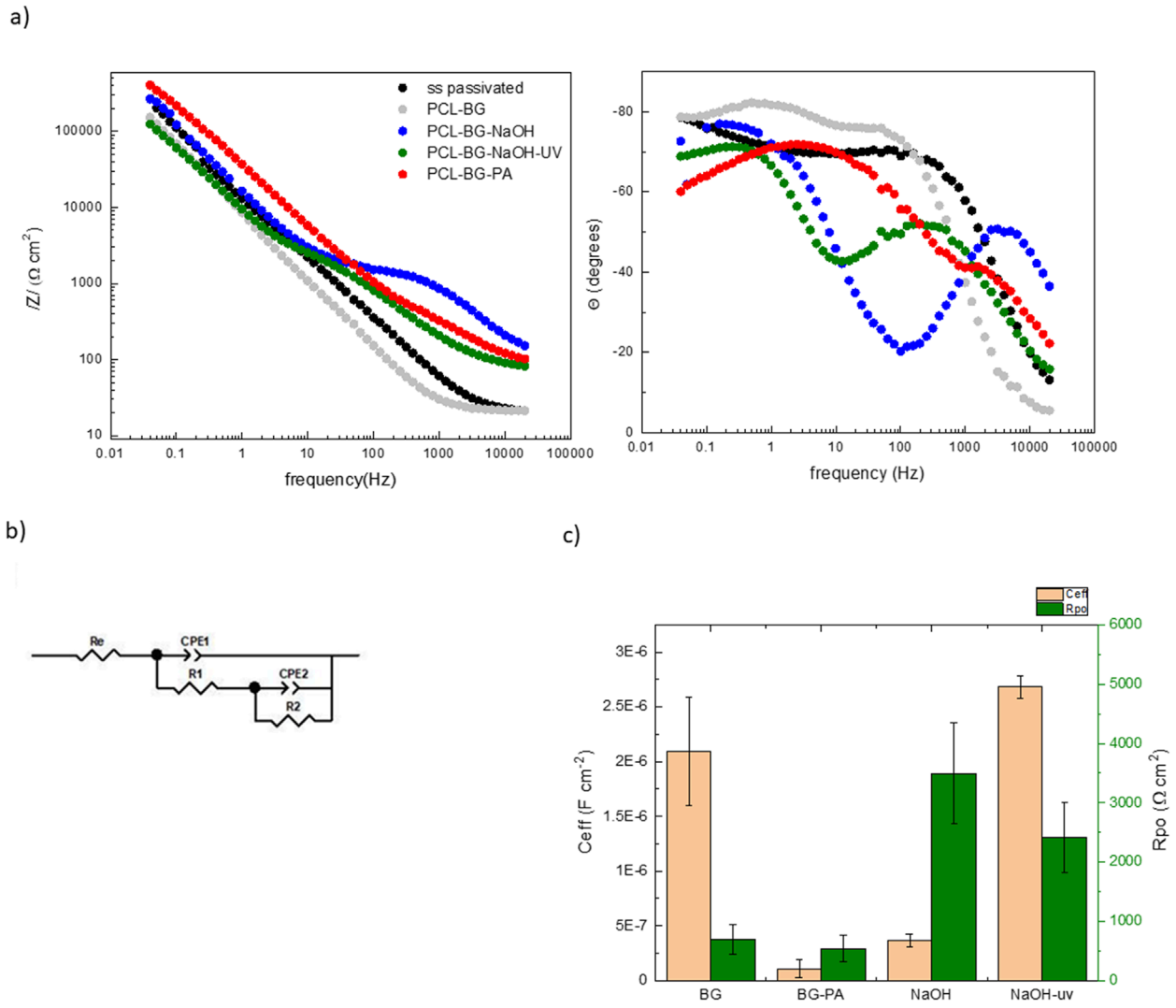

FIGURE 9
(A) Bode plots obtained in EIS study, **(B)** model used for the uncovered and the covered wires and **(C)** effective capacitance (Ceff) and Coating resistance (Rpo) obtained from EIS essay.

EDX mapping of the PCL + BG coating sample post-treated with NaOH (Figure 4) revealed the presence of Ca and Si from bioglass, thus corroborating their permanence within the fibers after the wet treatment.

FTIR spectra of the individual components and the hybrid coatings are shown in Figure 5. The main bands in the composite are obviously related to PCL bands, probably because the polymer is in a much larger relative concentration (Giannetti et al., 2019; Yang et al., 2015). PCL main bands include -CH_2 asymmetric and symmetric stretching vibrations around 2,943 and 2,864 cm^{-1}, carbonyl stretching at 1724 cm^{-1}, asymmetric and symmetric C–O–C stretching around 1,238 cm^{-1} and 1,163 cm^{-1} (Elzein et al., 2004), and the peak at 1,292 cm^{-1} due to C–O and C–C stretching (Liverani and Boccaccini, 2016). For the BG, the main bands are related to symmetric and antisymmetric Si–O–Si stretching at around 450 and 1,000 cm^{-1} respectively (Mačković et al., 2012) and Si–OH stretching around 1,000 cm^{-1} (Liverani et al., 2017). The main signals did not change after surface treatment, but a broad band was observed for the sample treated with PA and NaOH-UV, associated with - OH groups (stretching) in the region of 3,000–3,600 cm^{-1} (Jirofti et al., 2020). The FTIR spectrum of Eudragit EPO showed main bands at 1724 and 1,145 cm^{-1} related to carbonyl stretching vibrations and ester group stretching, respectively (Kielholz et al., 2022). The peaks related to amoxicillin were not detected in the coating probably because of the relatively low amount of the antibiotic compared to the polymer mass. After wet treatment, the FTIR spectra show no differences, although after being exposed to PBS with pH 5.5 (Supplementary Figure S3).

DSC results are depicted in Figure 6. Thermal analysis for the PCL + BG coating shows no differences in the composite melting temperature because of the surface post-treatments. Besides, the EEPO membrane shows a peak at 59.2°C related to its glass transition temperature, slightly higher than the values reported in other works (Abdelhakim et al., 2019). As a result of both thermal

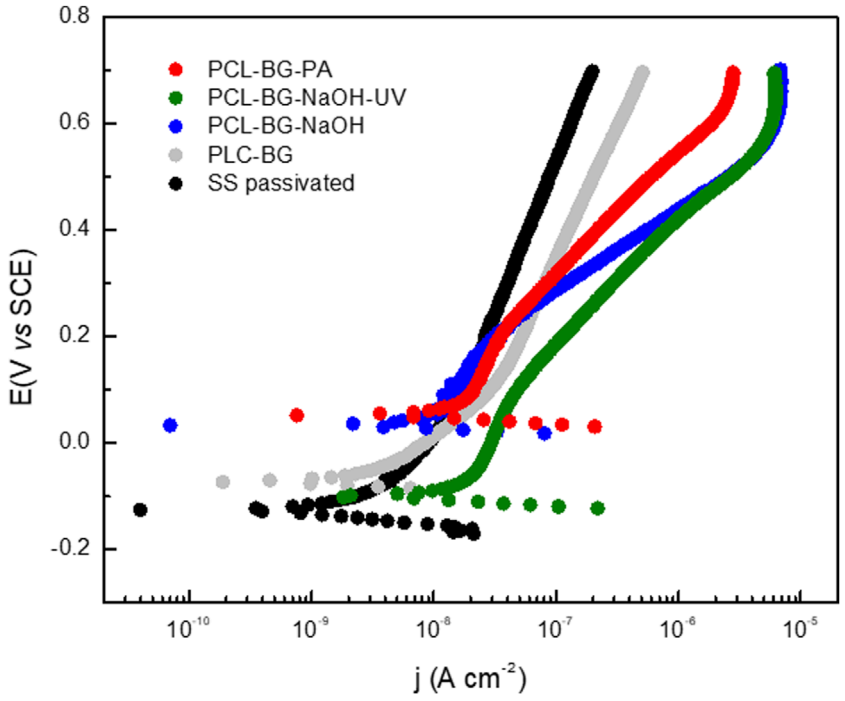

FIGURE 10
Potentiodynamic curves of the PCL-BG samples including the substrate. v = 0.001 V s^{-1}.

events being in the same temperature range, the co-electrospun coating exhibits a single peak at about 60.0°C (Figure 6). Besides, the melting enthalpy was slightly higher in the sample treated with PA, evidencing an increase in the crystallinity degree (from χ_c = 54.6%–58.8%), while it slightly decreased in the sample treated with NaOH-UV (χ_c = 53.8%).

Comparative TGA curves for the coatings are shown in Figure 7. Neat PCL thermogram exhibited a well-known main weight loss step between 350°C and 410°C, with a temperature of the maximum degradation rate at 399°C (Sergi et al., 2020). An important reduction in thermal stability of the composite coatings was observed, as the maximum polymer degradation rate was at 333°C for PCL + BG; probably caused by the effect of the fill which catalyzes the polymer thermal degradation (Merino and Alvarez, 2020; Larrañaga and Sarasua, 2013). Liverani et al. (2022) highlighted that the presence of water molecules in bioglass promotes an ester hydrolysis while PCL and the surface Si-O groups of bioglass may react as well. On the other hand, PA post-processing treatment caused a slight decrease in the temperature of maximum degradation rate (PCL + BG/PA: 316°C), which was not observed for the PCL + BG/NaOH + UV sample. For both post-treatments, a higher initial loss weight between 35°C and 200°C was observed when compared with the untreated sample, attributable to water loss and in good agreement with the hydrophilic character achieved with the surface treatments. Despite the absence of evident BG particles in the inspected surface of the treated coatings, the residual mass at 800°C is practically the same for PCL + BG and PCL + BG/PA, but a certain decrease was detected in PCL + BG/NaOH + UV related to some loss of BG. Then, according to TGA results, the successful incorporation of almost 3 wt% of BG into the fibers (compared to the 5 wt% added in the polymer solution before electrospinning) was achieved when processing over a cylindrical geometry. Although the PA wet treatment did not modify this value, the combined protocol based on NaOH + UV caused a higher loss of BG (around 1.5% left). The co-electrospun coating exhibited a 4.1% of residual mass at 800°C. A variation in the amount of BG with respect to the initial amount added in the polymeric solution was also observed in previous works (Sergi et al., 2020; Ródenas-Rochina et al., 2013). On the other hand, the thermal degradation of the coating composed only of EEEPO + AMX exhibits a weight loss that started at 250°C with a maximum degradation rate at 400°C, as well as the PCL + BG/EEPO + AMX.The encapsulation efficiency of AMX in EEPO fibers determined by UV-vis test was performed in triplicate, leading to a value of 94.3% ± 1.53.

3.3 Antibacterial effect

Eudragit E is a cationic copolymer that is insoluble in basic and neutral media but soluble at pH 5 or lower. In this study, EEPO fibers were used as carriers for amoxicillin to trigger a responsive release in the event of local acidification, which commonly occurs during bacterial infection.

Upon the onset of an infection, amoxicillin is expected to be released due to the dissolution of the EEPO fibers containing it. Accordingly, the study evaluated the antibacterial properties of the implant under neutral and acidic pH conditions. As shown in Figure 8, bacterial growth for both types of bacteria did not differ from the blank at pH 7, indicating that AMX was not released. However, under acidic conditions, there was

a noticeable impact on bacterial growth in samples containing AMX, with variations observed between the two types of bacteria. The antibacterial effect on *E. coli* was observed for up to 6 h, diminishing thereafter. For *S. aureus*, the effect was strongly noticeable after 24 and 48 h. The differences in behavior between the two bacterial types can be attributed to variations in outer membrane (OM) thickness and structure (Ballarre et al., 2023). The OM of Gram-negative bacteria like *E.coli* is considered a resistance determinant, as it acts as a barrier against various molecules due to its asymmetrical lipid bilayer. Additionally, Gram-negative bacteria possess a range of efflux pumps that can transport toxic molecules out of the cell (Saxena et al., 2023). This may explain why, under acidic conditions, released amoxicillin only delayed *E. coli* growth during the initial hours of cultivation, with the effect diminishing during later stages (stationary growth phase), likely due to activation of other defense mechanisms typical of Gram-negative microorganisms. In contrast, Gram-positive bacteria such as *S. aureus* lack this lipid layer, making their cells more permeable to antibiotics. This explains the higher sensitivity and sustained antibacterial effect observed for *S. aureus* under acidic conditions (24 and 48 h).

3.4 Electrochemical essays of PCL-based coatings

As the EEPO + AMX fibres would be lost after bacterial infection, the corrosion response of the coating consisting only of PCL + BG fibers was analysed. Electrospun coatings exhibit a porous interconnected microstructure that could eventually affect the corrosion behavior of the substrate. However, EIS analysis showed that the PCL + BG coating did not modify the EIS response of the passivated stainless steel. In Figure 9A it can be noticed that the curves of Z modulus for the substrate and PCL + BG were similar in all the frequency range. In general, it is accepted that the high-frequency region in the EIS results contains coating information while the low-frequency region contains information about the processes related to reactions on the electrode surface (Kim et al., 2017). The high frequency domain showed that phase angle did not reach zero in the coated samples, meaning that the coating is present on the substrate and that the treated coating could improve the corrosion resistance (Figure 9A) (Kim et al., 2017; Nasiriardali et al., 2022). However, the open structure was evident in the PCL + BG/NaOH and PCL + BG/NaOH + UV coatings where two-time constants in the phase angle vs. frequency plot were present, due to the electrolyte permeation into the coating, and in good agreement with the hydrophilic nature of the film. Nevertheless, a slight increase in total impedance was observed in all the frequency range, in the analyzed immersion times.

Equivalent circuits were proposed for the wires (Figure 9B) to simulate the corrosion response. Constant phase elements (CPE) were used to represent a "leaky capacitor" and the inhomogeneity of the surface. In the circuit, the R1 is in series with a solution resistance Re and represents the resistant of the electrolyte into the pores of membrane deposited on the surface. CPE1 is a constant phase element corresponding to the total oxide/membrane capacitance and CPE2 describes the inner layer of the surface membrane, between the bottom of the pores and the metal substrate. R2 is associated with the resistance of the inner oxide layer in contact with the metal.

The impedance for a CPE can be calculated as depicted in Equation 2, where Q and α are the pseudo capacitance and the deviation parameter respectively for the impedance of the CPE (Equation 2). When α = 1, Q represents an ideal capacitor.

$$Z_{CPE} = \frac{1}{Q(j\omega)^{\alpha}} \tag{2}$$

For a parallel array between a resistance and a CPE, the impedance can be calculated as follows (Equation 3).

$$Z_{R//CPE} = \frac{R}{1 + QR(j\omega)^{\alpha}} \tag{3}$$

Then, the CPE can be related to an "effective capacitance" (C_{eff}) considering a symmetric distribution of relaxation time. C_{eff} can be calculated as (Equation 4).

$$C_{eff} = \frac{(QR)^{1/\alpha}}{R} \tag{4}$$

Figure 9C shows the C_{eff} values obtained for the high frequency part of the impedance spectra in order to evaluate film capacitance.

The values obtained for the C_{eff} varied between 2.09 × 10^{-6} F cm^{-2} for PLC + BG to 3.7 × 10^{-7} F cm^{-2} for PCL + BG/NaOH. The reduction in the capacitance is associated with a more isolating membrane, together with the increase in the R1 value, related with the resistance to the electrolyte in the pores of the membrane. The C_{eff} increased and the R_{po} (R1) decreased after the UV treatment probably because of the more hydrophilic nature of the coating.

Figure 10 shows the potentiodynamic curves for the PCL + BG treated and untreated coated wires and the passivated substrate after 2 h of immersion in SBF at 37°C. All the coatings but the ones treated with NaOH presented corrosion current densities around 10^{-9} A cm^{-2}. The surface treatment with PA and NaOH produced an anodic shift in the corrosion potential probably due to an increase in the cathodic reaction kinetics. This agrees with the results of EIS where the appearance of two-time constants revealed the coating permeation and hence the electrolyte contact with the base material. The treatment with NaOH and UV increased the corrosion process compared with the passive substrate moving both anodic and cathodic branches. The permeation of the electrolyte through the coating was evident as observed in the EIS results.

4 Conclusion

In this study, we successfully developed and applied a novel device setup for electrospinning and co-electrospinning, enabling the creation of biomimetic coatings on cylindrical stainless steel wires. For the first time, these coatings were manufactured in a cylindrical geometry, offering significant advantages for *in vivo* testing with hybrid orthopedic implants in rat models. Our approach allowed us to incorporate bioglass into poly(ε-caprolactone) (PCL) fibers and verify its retention through two types of wet post-treatments. We observed that both acidic and basic/UV surface modifications significantly enhanced the hydrophilicity of the

coatings, with notable differences in the fibrous morphologies and composite compositions. By integrating antibiotic-loaded nanofibers via co-electrospinning, we provided a smart, responsive coating that effectively targets bacterial infections while preserving the structural integrity of the fibers. Remarkably, despite the interconnected porosity of the electrospun layers, the corrosion resistance of the coated materials remained uncompromised.

This study achieves three critical objectives: (Ballarre et al., 2013): it fills a significant research gap by demonstrating the successful manufacture of cylindrical composite electrospun coatings, paving the way for advanced *in vitro* assessment and *in-vivo* implant testing; (Trzaskowska et al., 2020); it evaluates various experimental protocols for the essential sterilization and disinfection of implants, offering practical insights for their final application; and (Stewart et al., 2019) it underscores the potential of these composite hybrid coatings and manufacturing techniques in advancing the field of bone tissue engineering.

Data availability statement

The original contributions presented in the study are included in the article/Supplementary Material, further inquiries can be directed to the corresponding author.

Author contributions

GK: Conceptualization, Formal Analysis, Investigation, Methodology, Writing–original draft. GR: Conceptualization, Formal Analysis, Supervision, Visualization, Writing–review and editing. JB: Conceptualization, Validation, Writing–review and editing. KH: Writing–review and editing, Investigation, Methodology. SC: Conceptualization, Formal Analysis, Supervision, Validation, Writing–review and editing. GA: Conceptualization, Supervision, Writing–review and editing, Funding acquisition, Project administration.

Funding

The author(s) declare that financial support was received for the research, authorship, and/or publication of this article. Consejo Nacional de Investigaciones Científicas y Técnicas (CONICET, PUE 2016-73), Agencia Nacional de Promoción Científica y Tecnológica (ANPCyT, grant PICT-2018-02334, PICT-2018-1157), Universidad Nacional de Mar del Plata (Project 15-G600).

Acknowledgments

The authors gratefully acknowledge the financial support provided by the Consejo Nacional de Investigaciones Científicas y Técnicas, the Agencia Nacional de Promoción Científica y Tecnológica and the Universidad Nacional de Mar del Plata.

Conflict of interest

The authors declare that the research was conducted in the absence of any commercial or financial relationships that could be construed as a potential conflict of interest.

Publisher's note

All claims expressed in this article are solely those of the authors and do not necessarily represent those of their affiliated organizations, or those of the publisher, the editors and the reviewers. Any product that may be evaluated in this article, or claim that may be made by its manufacturer, is not guaranteed or endorsed by the publisher.

Supplementary material

The Supplementary Material for this article can be found online at: https://www.frontiersin.org/articles/10.3389/fmats.2024.1484465/full#supplementary-material

References

Abdelhakim, H. E., Coupe, A., Tuleu, C., Edirisinghe, M., and Craig, D. Q. M. (2019). Electrospinning Optimization of Eudragit e PO with and without Chlorpheniramine Maleate Using a Design of Experiment Approach. *Mol. Pharm.* 16 (6), 2557–2568. doi:10.1021/acs.molpharmaceut.9b00159

Adhikari, J., Saha, P., and Sinha, A. (2018). "Surface modification of metallic bone implants-Polymer and polymer-assisted coating for bone in-growth," in *Fundamental biomaterials: metals*. Editors P. Balakrishnan, M. S. Sreekala, and T. Sabu (Sawston, United Kingdom: Woodhead Publishing), 299–321. doi:10.1016/B978-0-08-102205-4.00014-3

Bagde, A. D., Kuthe, A. M., Quazi, S., Gupta, V., Jaiswal, S., Jyothilal, S., et al. (2019). State of the art technology for bone tissue engineering and drug delivery. *Irbm* 40 (3), 133–144. doi:10.1016/j.irbm.2019.03.001

Bakhsheshi-Rad, H. R., Fauzi, A., Aziz, M., Hadisi, Z., Omidi, M., and Chen, X. (2019). Antibacterial activity and corrosion resistance of Ta_2O_5 thin film and electrospun PCL/MgO-Ag nano fiber coatings on biodegradable Mg alloy implants. *Ceram. Int.* 45, 11883–11892. doi:10.1016/j.ceramint.2019.03.071

Bakhsheshi-Rad, H. R., Hamzah, E., Abbasizadeh, N., Najafinezhad, A., and Kashefian, M. (2018). Synthesis of novel nanostructured bredigite–amoxicillin scaffolds for bone defect treatment: cytocompatibility and antibacterial activity. *J. Solgel Sci. Technol.* 86 (1), 83–93. doi:10.1007/s10971-018-4606-1

Ballarre, J., Buldain, D., Unalan, I., Pastore, J. I., Mestorino, N., and Boccaccini, A. R. (2023). Melaleuca armillaris essential oil as an antibacterial agent: the use of mesoporous bioactive glass nanoparticles as drug carrier. *Nanomaterials* 13 (1), 34. doi:10.3390/nano13010034

Ballarre, J., Desimone, P. M., Chorro, M., Baca, M., Carlos, J., and Ceré, S. M. (2013). Bone quality around bioactive silica-based coated stainless steel implants: analysis by Micro-Raman, XRF and XAS techniques. *J. Struct. Biol.* 184 (2), 164–172. doi:10.1016/j.jsb.2013.09.016

Bhaskaran, A., Prasad, T., Kumary, T. V., and Anil Kumar, P. R. (2019). Simple and efficient approach for improved cytocompatibility and faster degradation of electrospun polycaprolactone fibers. *Polym. Bull.* 76 (3), 1333–1347. doi:10.1007/s00289-018-2442-7

Chaiarwut, S., Ekabutr, P., Chuysinuan, P., Chanamuangkon, T., and Supaphol, P. (2021). Surface immobilization of PCL electrospun nanofibers with pexiganan for wound dressing. *J. Polym. Res.* 28 (9), 344. doi:10.1007/s10965-021-02669-w

Chen, F., Lee, C. N., and Teoh, S. H. (2007). Nanofibrous modification on ultra-thin poly(e-caprolactone) membrane via electrospinning. *Mater. Sci. Eng. C* 27 (2), 325–332. doi:10.1016/j.msec.2006.05.004

Cicuéndez, M., Doadrio, J. C., Hernández, A., Portolés, M. T., Izquierdo-Barba, I., and Vallet-Regí, M. (2018). Multifunctional pH sensitive 3D scaffolds for treatment and prevention of bone infection. *Acta Biomater.* 65, 450–461. doi:10.1016/j.actbio.2017.11.009

Dabirian, F., Ravandi, S. A. H., Hinestroza, J. P., and Abuzade, R. A. (2012). Conformal coating of yarns and wires with electrospun nanofibers. *Polym. Eng. Sci.* 52 (8), 1724–1732. doi:10.1002/pen.23109

Elzein, T., Nasser-Eddine, M., Delaite, C., Bistac, S., and Dumas, P. (2004). FTIR study of polycaprolactone chain organization at interfaces. *J. Colloid Interface Sci.* 273 (2), 381–387. doi:10.1016/j.jcis.2004.02.001

Giannetti, R., Abraham, G. A., and Rivero, G. (2019). The role of emulsion parameters in tramadol sustained-release from electrospun mats. *Mater. Sci. Eng. C* 99, 1493–1501. doi:10.1016/j.msec.2019.02.085

Haimi, S., Vienonen, A., Hirn, M., Pelto, M., Virtanen, V., and Suuronen, R. (2008). The effect of chemical cleansing procedures combined with peracetic acid-ethanol sterilization on biomechanical properties of cortical bone. *Biologicals* 36 (2), 99–104. doi:10.1016/j.biologicals.2007.06.001

Hanas, T., Sampath Kumar, T. S., Perumal, G., Doble, M., and Ramakrishna, S. (2018). Electrospun PCL/HA coated friction stir processed AZ31/HA composites for degradable implant applications. *J. Mater Process Technol.* 252, 398–406. doi:10.1016/j.jmatprotec.2017.10.009

Horakova, J., Klicova, M., Erben, J., Klapstova, A., Novotny, V., Behalek, L., et al. (2020). Impact of various sterilization and disinfection techniques on electrospun poly-ϵ-caprolactone. *ACS Omega* 5 (15), 8885–8892. doi:10.1021/acsomega.0c00503

Jirofti, N., Mohebbi-Kalhori, D., and Masoumi, R. (2020). Enhancing biocompatibility of PCL/PU nano-structures to control the water wettability by NaOH hydrolysis treatment for tissue engineering applications. *J. Industrial Text.* 51, 3278S–3296S. doi:10.1177/1528083720963268

Jokar, M., Darvishi, S., Torkaman, R., Kharaziha, M., and Karbasi, M. (2016). Corrosion and bioactivity evaluation of nanocomposite PCL-forsterite coating applied on 316L stainless steel. *Surf. Coat. Technol.* 307, 324–331. doi:10.1016/j.surfcoat.2016.08.094

Katta, P. P., and Nalliyan, R. (2019). Corrosion resistance with self-healing behavior and biocompatibility of Ce incorporated niobium oxide coated 316L SS for orthopedic applications. *Surf. Coat. Technol.* 375, 715–726. doi:10.1016/j.surfcoat.2019.07.042

Kielholz, T., Walther, M., Jung, N., and Windbergs, M. (2022). Electrospun fibers loaded with antimicrobial peptides for treatment of wound infections. *Eur. J. Pharm. Biopharm.* 179, 246–255. doi:10.1016/j.ejpb.2022.09.014

Kim, J., Mousa, H. M., Park, C. H., and Kim, C. S. (2017). Enhanced corrosion resistance and biocompatibility of AZ31 Mg alloy using PCL/ZnO NPs via electrospinning. *Appl. Surf. Sci.* 396, 249–258. doi:10.1016/j.apsusc.2016.10.092

Kim, Y., Young, J., Hoon, G., Seo, J. hyuk, Ryu, H. seung, and Kim, G. (2019). 3D-printed PCL/bioglass (BGS-7) composite scaffolds with high toughness and cell-responses for bone tissue regeneration. *J. Industrial Eng. Chem.* 79, 163–171. doi:10.1016/j.jiec.2019.06.027

Kiran, A. S. K., Kumar, T. S., Perumal, G., Sanghavi, R., Doble, M., and Ramakrishna, S. (2018). Dual nanofibrous bioactive coating and antimicrobial surface treatment for infection resistant titanium implants. *Prog. Org. Coat.* 121, 112–119. doi:10.1016/j.porgcoat.2018.04.028

Kokubo, T., and Takadama, H. (2006). How useful is SBF in predicting *in vivo* bone bioactivity? *Biomaterials* 27 (15), 2907–2915. doi:10.1016/j.biomaterials.2006.01.017

Kurusu, R. S., and Demarquette, N. R. (2019). Surface modification to control the water wettability of electrospun mats. *Int. Mater. Rev.* 64 (5), 249–287. doi:10.1080/09506608.2018.1484577

Larrañaga, A., and Sarasua, J. R. (2013). Effect of bioactive glass particles on the thermal degradation behaviour of medical polyesters. *Polym. Degrad. Stab.* 98 (3), 751–758. doi:10.1016/j.polymdegradstab.2012.12.015

Li, L. L., Wang, L. ming, Xu, Y., and Lv, L. xin (2012). Preparation of gentamicin-loaded electrospun coating on titanium implants and a study of their properties *in vitro*. *Arch. Orthop. Trauma Surg.* 132, 897–903. doi:10.1007/s00402-012-1490-y

Li, L. Y., Cui, L. Y., Zeng, R. C., Li, S. Q., Chen, X. B., Zheng, Y., et al. (2018). Advances in functionalized polymer coatings on biodegradable magnesium alloys – a review. *Acta Biomater.* 79, 23–36. doi:10.1016/j.actbio.2018.08.030

Lin, X., Su, L., Li, N., Hu, Y., Tang, G., Liu, L., et al. (2018). Understanding the mechanism of dissolution enhancement for poorly water-soluble drugs by solid dispersions containing Eudragit®E PO. *J. Drug Deliv. Sci. Technol.* 48, 328–337. doi:10.1016/j.jddst.2018.10.008

Liu, P., Xu, G., Pranantyo, D., Xu, L. Q., Neoh, K. G., and Kang, E. T. (2018). PH-sensitive zwitterionic polymer as an antimicrobial agent with effective bacterial targeting. *ACS Biomater. Sci. Eng.* 4 (1), 40–46. doi:10.1021/acsbiomaterials.7b00723

Liverani, L., and Boccaccini, A. R. (2016). Versatile production of poly(Epsilon-caprolactone) fibers by electrospinning using benign solvents. *Nanomaterials* 6 (4), 75. doi:10.3390/nano6040075

Liverani, L., Boccardi, E., Beltran, A. M., and Boccaccini, A. R. (2017). Incorporation of calcium containing mesoporous (MCM-41-type) particles in electrospun PCL fibers by using benign solvents. *Polym. (Basel)* 9 (10), 417. doi:10.3390/polym9100487

Liverani, L., Lacina, J., Roether, J. A., Boccardi, E., Killian, M. S., Schmuki, P., et al. (2018). Incorporation of bioactive glass nanoparticles in electrospun PCL/chitosan fibers by using benign solvents. *Bioact. Mater* 3 (1), 55–63. doi:10.1016/j.bioactmat.2017.05.003

Liverani, L., Liguori, A., Zezza, P., Gualandi, C., Toselli, M., Boccaccini, A. R., et al. (2022). Nanocomposite electrospun fibers of poly(ε-caprolactone)/bioactive glass with shape memory properties. *Bioact. Mater* 11, 230–239. doi:10.1016/j.bioactmat.2021.09.020

Mačković, M., Hoppe, A., Detsch, R., Mohn, D., Stark, W. J., Spiecker, E., et al. (2012). Bioactive glass (type 45S5) nanoparticles: *in vitro* reactivity on nanoscale and biocompatibility. *J. Nanoparticle Res.* 14, 966. doi:10.1007/s11051-012-0966-6

McFetridge, P. S., Daniel, J. W., Bodamyali, T., Horrocks, M., and Chaudhuri, J. B. (2004). Preparation of porcine carotid arteries for vascular tissue engineering applications. *J. Biomed. Mater Res. A* 70 (2), 224–234. doi:10.1002/jbm.a.30060

Merino, D., and Alvarez, V. A. (2020). Thermal degradation of poly (ε-caprolactone) nanocomposites with soy lecithin-modified bentonite fillers. *Thermochim. Acta* 689 (April), 178638. doi:10.1016/j.tca.2020.178638

Mouthuy, P. A., Zargar, N., Hakimi, O., Lostis, E., and Carr, A. (2015). Fabrication of continuous electrospun filaments with potential for use as medical fibres. *Biofabrication* 7 (2), 025006–025013. doi:10.1088/1758-5090/7/2/025006

Nasiriardali, M., Boroujeny, B. S., Doostmohammadi, A., Nazari, H., and Akbari, E. (2022). Improvement of biological and corrosion behavior of 316 L stainless steel using PDMS-Ag doped Willemite nanocomposite coating. *Prog. Org. Coat.* 165, 106733. doi:10.1016/j.porgcoat.2022.106733

Omar, S., Pellice, S., Ballarre, J., and Ceré, S. (2015). Hybrid organic-inorganic silica-based coatings deposited by spray technique. *Procedia Mater. Sci.* 9, 469–476. doi:10.1016/j.mspro.2015.05.018

Pawłowski, Ł., Bartmański, M., Mielewczyk-Gryń, A., Cieślik, B. M., Gajowiec, G., and Zieliński, A. (2021). Electrophoretically deposited chitosan/eudragit e 100/agnps composite coatings on titanium substrate as a silver release system. *Materials* 14 (16), 4533. doi:10.3390/ma14164533

Prabhakaran, M. P., Venugopal, J., and Ramakrishna, S. (2009). Electrospun nanostructured scaffolds for bone tissue engineering. *Acta Biomater.* 5 (8), 2884–2893. doi:10.1016/j.actbio.2009.05.007

Preem, L., Vaarmets, E., Meos, A., Jõgi, I., Putrinš, M., Tenson, T., et al. (2019). Effects and efficacy of different sterilization and disinfection methods on electrospun drug delivery systems. *Int. J. Pharm.* 567, 118450. doi:10.1016/j.ijpharm.2019.118450

Ródenas-Rochina, J., Ribelles, J. L. G., and Lebourg, M. (2013). Comparative study of PCL-HAp and PCL-bioglass composite scaffolds for bone tissue engineering. *J. Mater Sci. Mater Med.* 24 (5), 1293–1308. doi:10.1007/s10856-013-4878-5

Saxena, D., Maitra, R., Bormon, R., Czekanska, M., Meiers, J., Titz, A., et al. (2023). Tackling the outer membrane: facilitating compound entry into Gram-negative bacterial pathogens. *npj Antimicrob. Resist.* 1 (1), 17. doi:10.1038/s44259-023-00016-1

Sergi, R., Cannillo, V., Boccaccini, A. R., and Liverani, L. (2020). Incorporation of bioactive glasses containing Mg, Sr, and Zn in electrospun PCL fibers by using benign solvents. *Appl. Sci. Switz.* 10 (16), 5530. doi:10.3390/app10165530

Son, Y. J., Kim, Y., Kim, W. J., Jeong, S. Y., and Yoo, H. S. (2015). Antibacterial nanofibrous mats composed of eudragit for pH-dependent dissolution. *J. Pharm. Sci.* 104 (8), 2611–2618. doi:10.1002/jps.24521

Soujanya, G. K., Hanas, T., Chakrapani, V. Y., Sunil, B. R., and Kumar, T. S. S. (2014). Electrospun nanofibrous polymer coated magnesium alloy for biodegradable implant applications. *Procedia Mater. Sci.* 5, 817–823. doi:10.1016/j.mspro.2014.07.333

Stewart, C., Akhavan, B., Wise, S. G., and Bilek, M. M. M. (2019). A review of biomimetic surface functionalization for bone-integrating orthopedic implants: mechanisms, current approaches, and future directions. *Prog. Mater Sci.* 106, 100588. doi:10.1016/j.pmatsci.2019.100588

Su, Y., Luo, C., Zhang, Z., Hermawan, H., Zhu, D., Huang, J., et al. (2018). Bioinspired surface functionalization of metallic biomaterials. *J. Mech. Behav. Biomed. Mater* 77, 90–105. doi:10.1016/j.jmbbm.2017.08.035

Tao, B., Deng, Y., Song, L., Ma, W., Qian, Y., Lin, C., et al. (2019). BMP2-loaded titania nanotubes coating with pH-responsive multilayers for bacterial infections inhibition and osteogenic activity improvement. *Colloids Surf. B Biointerfaces* 177, 242–252. doi:10.1016/j.colsurfb.2019.02.014

Trzaskowska, P. A., Poniatowska, A., Tokarska, K., Wiśniewski, C., Ciach, T., and Malinowska, E. (2020). Promising electrodeposited biocompatible coatings for steel obtained from polymerized microemulsions. *Colloids Surf. A Physicochem Eng. Asp.* 591, 124555. doi:10.1016/j.colsurfa.2020.124555

Yalcinkaya, F. (2019). Preparation of various nanofiber layers using wire electrospinning system. *Arabian J. Chem.* 12 (8), 5162–5172. doi:10.1016/j.arabjc.2016.12.012

Yang, Y., Michalczyk, C., Singer, F., Virtanen, S., and Boccaccini, A. R. (2015). *In vitro* study of polycaprolactone/bioactive glass composite coatings on corrosion and bioactivity of pure Mg. *Appl. Surf. Sci.* 355, 832–841. doi:10.1016/j.apsusc.2015.07.053

Yew, C. H. T., Azari, P., Choi, J. R., Muhamad, F., and Pingguan-Murphy, B. (2018). Electrospun polycaprolactone nanofibers as a reaction membrane for lateral flow assay. *Polym. (Basel)* 10 (12), 1387. doi:10.3390/polym10121387

Yoganarasimha, S., Trahan, W. R., Best, A. M., Bowlin, G. L., Kitten, T. O., Moon, P. C., et al. (2014). Peracetic acid: a practical agent for sterilizing heat-labile polymeric tissue-engineering scaffolds. *Tissue Eng. Part C Methods* 20 (9), 714–723. doi:10.1089/ten.tec.2013.0624